

Spatial-Temporal Motion Control via Composite Cam-follower Mechanisms

YINGJIE CHENG, University of Science and Technology of China, China and Singapore University of Technology and Design, Singapore

YUCHENG SUN, University of Science and Technology of China, China and Singapore University of Technology and Design, Singapore

PENG SONG*, Singapore University of Technology and Design, Singapore

LIGANG LIU, University of Science and Technology of China, China

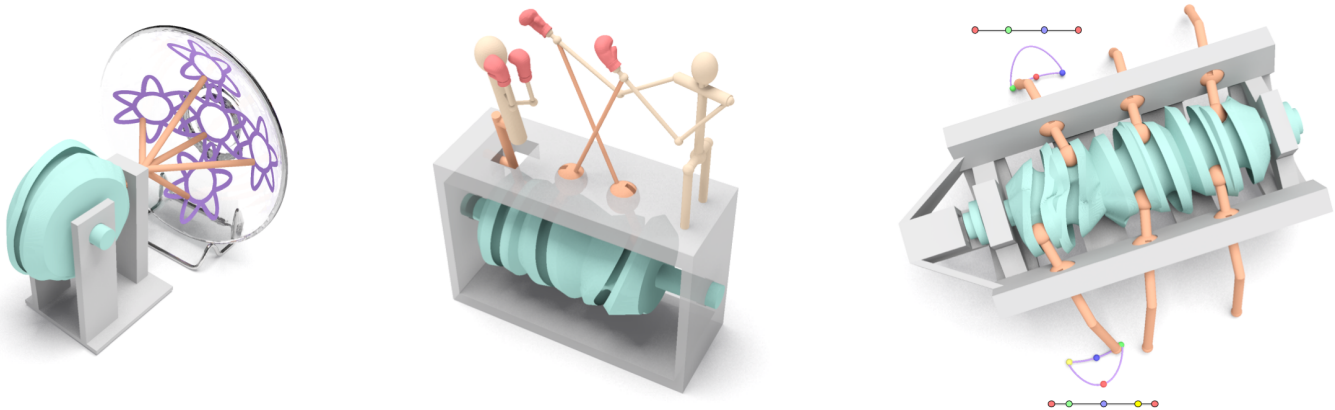


Fig. 1. We present a computational technique to model, design, and optimize composite cam-follower mechanisms for personalized automata, and showcase our technique on a diverse set of examples including (from left to right): drawing on a non-planar surface, displaying realistic toy motion, and walking according to a user-specified gait. Our technique enables users to control an automaton's spatial-temporal motion by specifying the target trajectories and timings (see the two spatial curves and corresponding time sliders in the right example).

Motion control, both on the trajectory and timing, is crucial for mechanical automata to perform functionalities such as walking and entertaining. We present *composite cam-follower mechanisms* that can control their spatial-temporal motions to exactly follow trajectories and timings specified by users, and propose a computational technique to model, design, and optimize these mechanisms. The building blocks of our mechanisms are a new kind of cam-follower mechanism with a modified joint, in which the follower can perform spatial motion on a planar, cylindrical, or spherical surface controlled by the 3D cam's profile. We parameterize the geometry of these cam-follower mechanisms, formulate analytical equations to model their

kinematics and dynamics, and present a method to combine multiple cam-follower mechanisms into a working mechanism. Taking this modeling as a foundation, we propose a computational approach to designing and optimizing the geometry and layout of composite cam-follower mechanisms, with an objective of performing target spatial-temporal motions driving by a small motor torque. We demonstrate the effectiveness of our technique by designing different kinds of personalized automata and showing results not attainable by conventional mechanisms.

CCS Concepts: • Computing methodologies → Shape modeling; Physical simulation.

Additional Key Words and Phrases: cam-follower mechanism, kinematic modeling, computational design, 3D printing

ACM Reference Format:

Yingjie Cheng, Yucheng Sun, Peng Song, and Ligang Liu. 2021. Spatial-Temporal Motion Control via Composite Cam-follower Mechanisms. *ACM Trans. Graph.* 40, 6, Article 270 (December 2021), 15 pages. <https://doi.org/10.1145/3478513.3480477>

*The corresponding author

Authors' addresses: Yingjie Cheng, University of Science and Technology of China, China and Singapore University of Technology and Design, Singapore, chengyj@mail.ustc.edu.cn; Yucheng Sun, University of Science and Technology of China, China and Singapore University of Technology and Design, Singapore, syc1011@mail.ustc.edu.cn; Peng Song, Singapore University of Technology and Design, Singapore, peng_song@sutd.edu.sg; Ligang Liu, University of Science and Technology of China, China, lgl@ustc.edu.cn.

Permission to make digital or hard copies of all or part of this work for personal or classroom use is granted without fee provided that copies are not made or distributed for profit or commercial advantage and that copies bear this notice and the full citation on the first page. Copyrights for components of this work owned by others than ACM must be honored. Abstracting with credit is permitted. To copy otherwise, or republish, to post on servers or to redistribute to lists, requires prior specific permission and/or a fee. Request permissions from permissions@acm.org.

© 2021 Association for Computing Machinery.
0730-0301/2021/12-ART270 \$15.00
<https://doi.org/10.1145/3478513.3480477>

1 INTRODUCTION

Mechanical automata have been created for many different purposes since ancient times such as drawing machines and mechanical toys [Peppé 2002]. Now, the increasing accessibility of rapid manufacturing devices makes it possible to fabricate mechanical automata

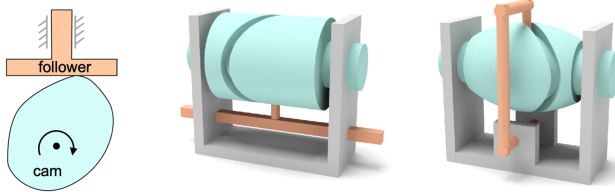


Fig. 2. Conventional cam-follower mechanisms with: (left) a plate, (middle) a cylindrical, and (right) a globoidal cam. Cams, followers, and supports are colored in cyan, orange, and gray respectively.

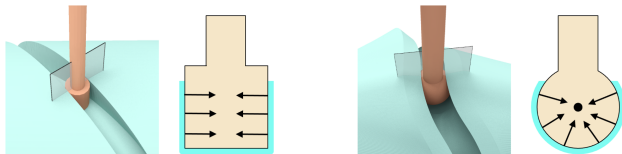


Fig. 3. Cam-follower joints modeled in conventional (left) and our (right) cam-follower mechanisms, where possible contact forces between the cam and the follower are shown as black arrows.

conveniently. To design mechanical automata according to individual needs and preferences, a number of computational methods and tools have been developed, focusing on constructing a mechanism that transfers a driving motion (e.g., from a motor or crank) to a user-desired periodic motion performed by an automaton.

Mechanisms designed by existing methods are typically a combination of linkages and gears [Ceylan et al. 2013; Coros et al. 2013; Roussel et al. 2018; Song et al. 2017; Thomaszewski et al. 2014]. These linkage-based mechanisms consist of a few parameters (e.g., joint position), which facilitates their design process yet also limits the space of motions that can be supported by them. Due to this reason, these mechanisms can approximate but not exactly follow a user-specified trajectory on a planar surface. And they rely on other mechanical parts such as non-circular gears to control the timing of the output motion [Coros et al. 2013].

In this paper, we aim to design mechanisms whose output motions can exactly follow user-specified trajectories and timings. Such mechanisms would offer users more control on the design process and enable designing automata with complex behavior. We choose cams and followers as building blocks to construct these mechanisms due to their strong capacity for precise and repeatable motion control [Abderazek et al. 2020]. Conventional cam-follower mechanisms, or simply *camMechs*, are insufficient for our goal since they, either with a plate cam or a 3D cam, can only output simple linear or oscillatory motion; see Figure 2. To this end, we model a new kind of *camMech*, in which the follower can perform complex spatial motion on a planar or non-planar surface precisely controlled by the 3D cam's profile. This is enabled by modeling the cam-follower joint as a *follower ball* moving in a cam groove. By this, the cam can push the follower along a much wider variety of directions through the curved-line contact, compared with the straight-line contact in conventional ones; see Figure 3.

To design a mechanical automaton, we take as input a network of smooth, closed curves that represent the target motion trajectories. To support timing control, users can specify a set of key points on each curve, and adjust the timing for each interval on the curve; see

Figure 1 (right) for an example. Our problem is to design a mechanism composed of *camMechs*, called *composite camMech* or simply *C-camMech*, that can transfer the rotational motion from a driving motor to realize the target spatial-temporal motions. To ensure that the *C-camMech* can be installed and used in the automaton, the mechanism should also satisfy several fabrication requirements, including lightweight, compact, and drivable by a small motor torque. Our problem is non-trivial since little is known about this new kind of *camMechs*, not to mention combining and optimizing them to form a working mechanism that satisfies our design objectives.

To address the challenge of designing *C-camMechs*, we make the following contributions:

- We present and classify a table of *camMechs* that can output spatial motions on a planar, cylindrical, or spherical surface, and propose a unified method to model their geometry, kinematics, and dynamics. We model a working *C-camMech* by connecting multiple *camMechs* following a tree structure.
- We propose a computational approach for the design and optimization of a *C-camMech* to produce spatial-temporal motions that exactly follow user-specified trajectories and timings. Our approach also optimizes for the geometry, layout, and required driven torque of the *C-camMech* to make it satisfy the fabrication requirements.

We have verified the kinematic performance of our designed *C-camMechs* with both simulated and physical experiments. The usefulness of our *C-camMechs* has been demonstrated in enabling a variety of functionalities of personalized automata that cannot be easily achieved by conventional mechanisms, including drawing free-form sketches on non-planar surfaces, displaying realistic toy motions, and walking following a user-specified gait; see Figure 1.

2 RELATED WORK

Mechanism modeling. Mechanism modeling concerns about geometry, motion, and functionality of existing mechanisms. The seminal work by Mitra et al. [2010] inferred motion of individual parts and their interactions based on the geometry of given mechanical assemblies. Later, Hergel et al. [2015] produced a functional 3D model from a 2D mechanism design for 3D fabrication while Ureta et al. [2016] created physically realizable joints in initial mechanical objects. Other researchers are interested in reconstructing a functional mechanism model that matches a real-world target represented by color images [Lin et al. 2018b; Xu et al. 2016] or depth scans [Lin et al. 2018a].

Mechanism design. In the era of digital fabrication, computational design of mechanisms for fabricating personalized automata has attracted great interest from the graphics community. A number of computational methods have been developed to address this challenging task, which can be classified into three classes according to the user input. The first class aims to design a mechanism that can reproduce periodic motion in a 3D animation [Zhu et al. 2012] or approximate a motion capture sequence of a humanoid character [Ceylan et al. 2013]. The second class focuses on designing mechanisms such that an automaton's pose can match user-specified keyframes as closely as possible, e.g., by using linkages [Megaro et al. 2014] or kinetic wires [Xu et al. 2018]. The third class aims to

Table 1. Classification of our camMechs according to the follower motion type allowed by its support.

	Example	Follower-support joint	Follower motion	v_s	Follower Trajectory
camMech_1T	Fig 4 (a)	prismatic joint	1-DOF translation	translation direction	3D line
camMech_1O	Fig 4 (b)	revolute joint	1-DOF oscillation	rotation axis	3D arc
camMech_1R	Fig 4 (c)	revolute joint	1-DOF rotation	rotation axis	3D circle
camMech_2T	Fig 4 (d)	(modified) sliding joint	2-DOF translation	normal of the translation plane	curve on a planar surface
camMech_1T1R	Fig 4 (e)	cylindrical joint	1-DOF translation & 1-DOF rotation	translation direction & rotation axis	curve on a cylindrical surface
camMech_2R	Fig 4 (f)	(modified) ball joint	2-DOF rotation	axis of the motion cone	curve on a spherical surface

approximate user-specified trajectories by designing and optimizing different kinds of mechanisms with gears and linkages [Bächer et al. 2015; Coros et al. 2013; Roussel et al. 2018; Thomaszewski et al. 2014], higher pair joints [Song et al. 2017], or compliant joints [Megaro et al. 2017; Tang et al. 2020].

Compared with the above works, our work is most similar to [Zhu et al. 2012] and [Coros et al. 2013]. Zhu et al. [2012] designed mechanical toys to reproduce motion trajectories and timings in a 3D animation. Their mechanisms rely on plate cams for spatial-temporal motion control, and thus mainly support linear or circular motion trajectories. In contrast, our C-camMechs make use of 3D cams to realize complex, free-form motion trajectories on both planar and non-planar surfaces. Coros et al. [2013] designed linkage-based mechanisms to approximate user-specified trajectories on a planar surface while our camMechs can exactly reproduce these trajectories. Our camMechs also support both planar and non-planar spatial motions, as well as allow exact timing control. One disadvantage of our camMechs is their bulky and complex 3D geometry, leading to more cost and higher demand on fabrication. See Section 7 and Figure 18 for a comparison experiment with more discussions.

Cam-follower mechanisms. A cam-follower mechanism or cam-Mech consists of a cam, a follower, and respective supports. The cam rotates periodically around a fixed axis to drive a specific kind of motion performed by the follower. A camMech can transfer planar (spatial) motion by using a plate (3D) cam; see again Figure 2. Plate cam mechanisms have been extensively studied and a variety of methods have been proposed to optimize their design for various purposes [Takahashi and Okuno 2018; Zhu et al. 2012]; see [Abderazek et al. 2020] for a review.

Spatial camMechs are characterized by a 3D cam and an ability to transfer spatial motion in full 3D space. These mechanisms have been successfully practiced in mechanical engineering [Chang et al. 2009] and robotics [Khan and Chen 2018; Koustoumpardis et al. 2017]. To design a spatial camMech, existing methods focus on constructing the groove surface of a 3D cam with analytical expressions such that the follower (with a given shape) can produce desired output motion. These methods can be classified into three classes, which are based on the screw theory, the theory of envelopes, and modeling swept surfaces, respectively. In the first approach [Chang et al. 2009; Dhande et al. 1975; González-Palacios and Angeles 1994], the screw theory is used to determine the condition of contact between the cam groove and the follower surface, based on which the instantaneous contact point/line on the follower surface can be computed. The cam groove surface is obtained by transforming

the instantaneous contact point/line within one motion period to the cam's coordinate system. In the second approach [Backhouse and Jones 1990; Hwang and Tsay 2009; Tsay and Hwang 1994; Tsay and Wei 1996], the cam groove surface is computed as an envelope for the family of the follower surfaces in different positions when the cam rotates for a complete cycle. In the third approach [Tsay and Lin 1996, 2006], the cam groove surface is computed as a swept surface of the follower in motion.

In all the above research works, the spatial camMechs output only linear or oscillatory motions. We only realize a recent creative work [Sugihara 2016] in which the spatial camMechs can output quasi-elliptical motions. In contrast, we model, simulate, and classify spatial camMechs that can perform free-form motion trajectories on both planar and non-planar surfaces, and optimize these camMechs to realize user-specified trajectories and timings for computational design of personalized automata.

3 PROBLEM DEFINITION

Our problem is to design a C-camMech that transfers the rotational motion of a driving motor to the periodic motions performed by an automaton's end-effectors according to the user input. In the following, we first define C-camMech, and then describe the user input and requirements for designing C-camMechs.

C-camMech. A C-camMech is a working mechanism composed of multiple camMechs, driven by a single motor with a motion period denoted as T . A C-camMech can output multiple motions simultaneously. The type of output motions supported by C-camMechs is determined by its component camMechs. We classify camMechs according to this output motion type as below.

We focus on camMechs with the ball-move-in-groove joint shown in Figure 3 (right). Thanks to this joint, the 3D cam can push the follower along both radial and axial directions, thus controlling at most 2 degrees of freedom (DOFs) of the follower. The actual type of motion performed by the follower is defined by the follower support. We classify the camMechs into six classes according to the follower motion type; see Table 1 and Figure 4. We name each class of camMechs as camMech_M, where M is the abbreviation of the follower's motion type. For example, camMechs whose follower motion is 1-DOF translation are named camMech_1T.

Among all the six classes, camMechs with 2-DOF follower motion (i.e., camMech_2T, camMech_1T1R, and camMech_2R) are unique from conventional ones since they support complex, free-form motion trajectories on a planar, cylindrical, or spherical surface, respectively. camMechs with 1-DOF follower motion (i.e., camMech_1T,

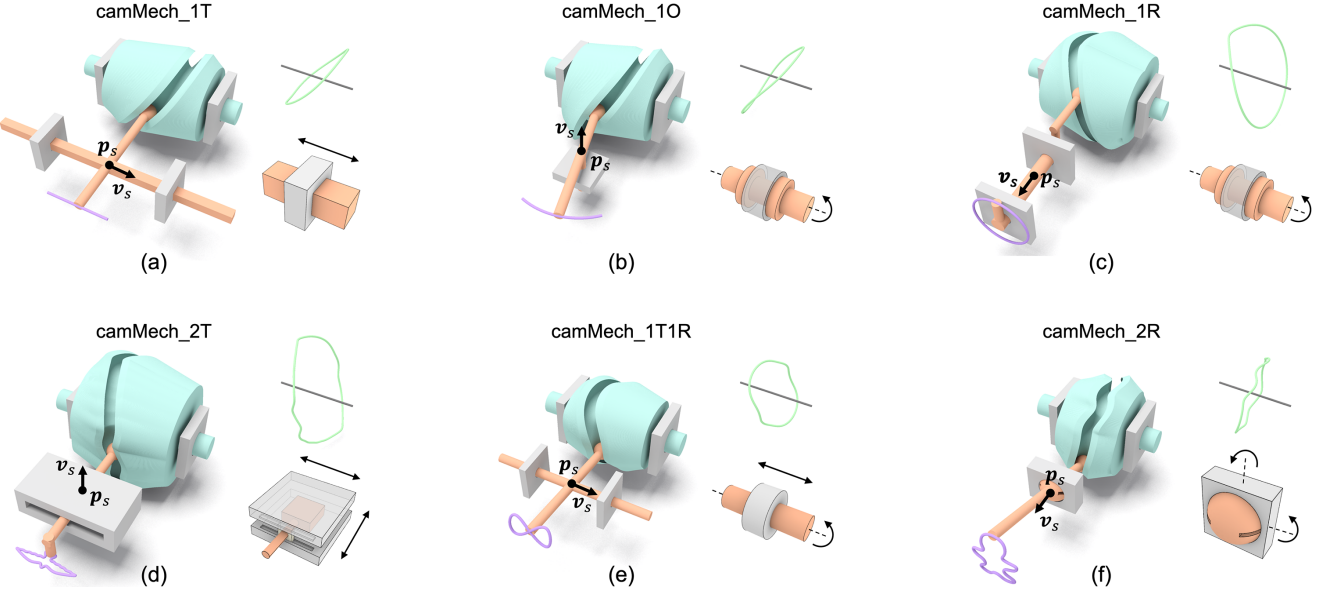
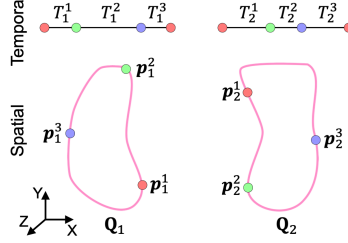


Fig. 4. Six classes of camMechs that we have modeled, where the follower can perform (a) 1-DOF translation, (b) 1-DOF oscillation, (c) 1-DOF rotation, (d) 2-DOF translation, (e) 1-DOF translation & 1-DOF rotation, and (f) 2-DOF rotation. For each camMech, the 3D cam's pitch curve and the follower trajectory are colored in green and purple respectively. The follower-support joint as well as its allowed motion are shown at the bottom right of each camMech.

Fig. 5. An example input of our approach, consisting of two curves, three key points (in red, green, and blue respectively) on each curve, and timing between each pair of adjacent key points (see the time slider on top of each curve).



camMech_1O, and camMech_1R) extend conventional ones by allowing adjusting the follower's translation direction or rotation axis relative to the 3D cam; see Figure 7. In addition, camMech_1R is specific in the sense that its output motion has the same type as the input motion. We will see in Section 5 how this characteristic of camMech_1R enables to connect camMechs in a chain manner.

User input. The user input includes m closed, smooth parametric curves $Q_k(u)$, $u \in [0, 1]$, $1 \leq k \leq m$ properly arranged in the 3D world space, where each curve represents the target trajectory of an end-effector; see Figure 5. For each input curve, we define $Q_k(0)$ as the end-effector's initial position at time $t = 0$. To enable timing control, users are allowed to insert n_k key points $\{p_k^l\}$, $1 \leq l \leq n_k$ on each curve $Q_k(u)$ following a certain order (i.e., either clockwise or counter-clockwise), where the first key point p_k^1 has to be at $Q_k(0)$ (see the red points in Figure 5). Users also need to specify a relative time interval between each pair of adjacent key points denoted as $\{T_k^l\}$, where $T_k^l > 0$ and $\sum_l T_k^l = 1$. If users want an end-effector to stop at a specific point on the curve for some time, they simply insert two key points at that location and specify desired timing for the interval between the two key points. When there are multiple end-effectors (e.g., two hands of a character, four legs of a robot),

synchronizing motions of these end-effectors by adjusting the input trajectories and timings would enable realistic and/or functional behavior (e.g., boxing, walking) of the automaton.

Design requirements. Given the user input, our designed C-camMech should satisfy the following high-level requirements:

- (1) *Motion trajectory.* The trajectories of an automaton's end-effectors should be exactly the same as the input curves $\{Q_k(u)\}$.
- (2) *Motion timing.* For each end-effector, it should pass through each key point p_k^l on the curve $Q_k(u)$ exactly at time $t = \sum_{j=1}^l T_k^j \cdot T$.
- (3) *Small driven torque.* The whole C-camMech should be drivable by a small torque provided by micromotors that are widely used for personalized automata.
- (4) *Lightweight mechanism.* The C-camMech should be lightweight to save fabrication cost as well as energy to drive it during usage.
- (5) *Compact mechanism.* The C-camMech should be compact such that it can be easily installed in an automaton.

To address the above design problem, we first present a unified approach to modeling geometry, kinematics, and dynamics of our camMechs (Section 4), and then a method to combine multiple camMechs into a working C-camMech by connecting them following a tree structure (Section 5). In Section 6, we describe our computational approach for the design and optimization of a C-camMech to satisfy the five high-level requirements described above. In particular, our optimization formulates the first two requirements on kinematics as hard constraints, aiming to make the output motions exactly follow the input trajectories and timings.

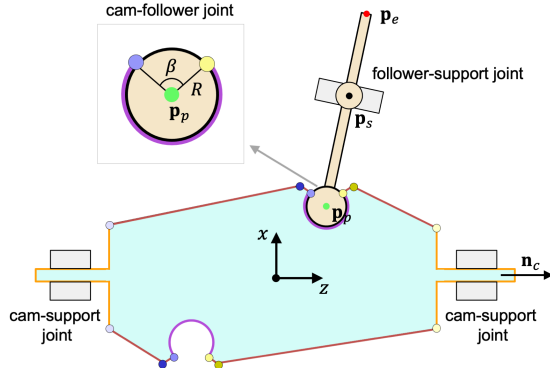


Fig. 6. A cross-section view of a camMech_2R, where we assume the cam rotation axis and the follower are coplanar for ease of illustration. The cam groove surface is represented as a purple arc, while the two boundary curves of the groove are represented as blue and yellow dots respectively. A zoom view of the cam-follower joint is shown on the top left.

4 MODELING CAM-FOLLOWER MECHANISMS

This section introduces a unified approach to modeling geometry, kinematics, and dynamics for the six classes of camMechs shown in Table 1 and Figure 4.

4.1 Geometric Modeling

Given a camMech, we define a local coordinate system in this way: the origin is at the middle point of the cam's rotation axis, the z -axis is the cam's rotation axis, and the x -axis is defined by the pose of the follower support relative to the cam; see Figure 6. Variables for geometry, kinematic, and dynamic modeling of the camMech are all defined in this coordinate system, unless otherwise specified.

Geometric modeling is about modeling geometry of three kinds of joints (i.e., cam-support joint, follower-support joint, cam-follower joint) and three kinds of parts (cam, follower, supports) in a camMech; see Figure 6. In particular, each of the cam, follower, and supports is just a piece of shape that holds respective joints, e.g., for fabrication; see Figure 4. In the following, we mainly describe how we model the joints and the cam.

i) *Cam-support joint* is modeled as a revolute joint, where the rod is integrated with the cam while the knuckle is fixed on the support. The cam can perform rotational motion periodically around a 3D axis \mathbf{n}_c defined by the support, which is the z -axis of the camMech coordinate system.

ii) *Follower-support joint* is modeled as a mechanical joint to support the follower motion for each class of camMechs. The third column from the left in Table 1 shows the names of these joints while the insets in Figure 4 show their geometry. In particular, camMech_2T uses a sliding joint while camMech_2R uses a ball joint, as the follower-support joint. A sliding joint typically allows 3-DOF motion (2-DOF translation and 1-DOF rotation) and a ball joint allows 3-DOF rotation. To support our 2-DOF follower motion, we modify the joints geometry to remove 1-DOF motion that we do not want, i.e., 1-DOF rotation for the sliding joint and 1-DOF rolling for the ball joint.



Fig. 7. The follower motion axis \mathbf{v}_s can deviate from its default direction (i.e., parallel with the cam axis for camMech_1T1R; see the dashed line) by a small angle α . From left to right, α equals 0, 20, and 40 degrees, respectively.

For each class of camMech, the position and orientation of the follower-support joint are defined by a point \mathbf{p}_s and a vector \mathbf{v}_s , respectively; see Figure 4. In particular, vector \mathbf{v}_s also defines the axis of follower motion for each camMech, e.g., translation direction for camMech_1T and rotation axis for camMech_1O; see Table 1 for details. By default, \mathbf{v}_s is parallel with one of the major axes of the camMech's local frame, as shown in Figure 4. To support more flexible follower motion, \mathbf{v}_s can deviate from its default direction by an angle α ; see Figure 7. In our design, we prefer a small deviation angle $\alpha < \alpha_{\text{thres}} = 45^\circ$, and choose $\alpha = 0$ whenever possible. This is because a larger deviation angle α will likely lead to worse dynamic performance of the camMech; see the supplementary material for details. Besides the pose, the geometry of the follower-support joint (e.g., the prismatic joint) should support the output motion range (e.g., 1-DOF translation), and relevant parameters are denoted as $\{J_{\text{geom}}\}$.

iii) *Cam-follower joint* is modeled as a ball-move-in-groove joint, where the ball is one end of the follower called the *follower ball* while the groove is part of the cam called the *cam groove*; see again Figure 3 (right). The radius and center point of the follower ball is denoted as R and \mathbf{p}_p respectively; see Figure 6. The cam groove is modeled as a tube (i.e., a swept surface) that envelops the follower ball when the follower moves relative to the cam. The tube has an opening described by an opening angle β (see the zoom view in Figure 6), through which the follower ball connects to the follower body without colliding with the cam.

The centerline of the cam groove is called the *pitch curve*, generated by the follower ball center \mathbf{p}_p as the follower moves relative to the cam. The pitch curve should be a closed, smooth, and non-self-intersecting 3D curve that surrounds the cam's rotation axis. We model the pitch curve with a parametric function $C(s) = (x(s), y(s), z(s))$, where s is a parameter in $[0, 1]$. In particular, we parameterize $C(s)$ in a way that $C(0)$ corresponds to the position of the follower ball center \mathbf{p}_p at time $t = 0$.

iv) *3D cam geometry*. Due to the opening, the cam groove has two closed boundary curves, represented as blue and yellow dots respectively; see the zoom view in Figure 6. The 3D cam geometry is modeled as a watertight surface that holds the groove surface in a way that the two boundary curves of the groove are exactly on the cam surface. To this end, for each boundary curve (e.g., the blue one), we generate two corresponding closed curves: a near big curve (e.g., the dark blue one) to make the groove structurally sound, and a further small curve (e.g., the light blue one) to define a side face of the cam. We linearly interpolate the three curves to form part

of the cam surface. The 3D cam geometry is obtained by stitching the two interpolated surfaces (in brown), the cam groove surface (in purple), and the two side surfaces (in orange); see Figure 6.

4.2 Kinematic Modeling

Both the cam and the follower perform periodic motion, and we denote their periods as T_c and T_f respectively. In this paper, we assume $T_c = T_f = T$ for simplicity, where T is the motion period of the motor that drives the cam. The goal of kinematic modeling is to determine the follower pose $\mathbf{O}_f(t)$ given the cam pose $\mathbf{O}_c(t)$ at any time $t \in [0, T]$.

The initial cam pose $\mathbf{O}_c(0)$ and follower pose $\mathbf{O}_f(0)$ are assumed to be known. We rewrite $\mathbf{O}_c(t) = \mathbf{T}_c(t)\mathbf{O}_c(0)$ and $\mathbf{O}_f(t) = \mathbf{T}_f(t)\mathbf{O}_f(0)$, where $\mathbf{T}_c(t)$ and $\mathbf{T}_f(t)$ are transforms applied on the cam and follower respectively. Hence, the kinematics of a camMech can be modeled as a transmission function:

$$\mathbf{T}_f(t) = K(\mathbf{T}_c(t)), \quad t \in [0, T] \quad (1)$$

At time $t > 0$, we assume that the cam has rotated around its axis \mathbf{n}_c for θ_c degrees from its initial pose. Then we have $\mathbf{T}_c(t) = \mathbf{R}(\mathbf{n}_c, \theta_c(t))$. Since the pitch curve $C(s)$ rotates together with the 3D cam, any point on this rotating pitch curve can be represented as $\mathbf{T}_c(t)C(s)$. Since the follower ball center \mathbf{p}_p is a point on the pitch curve, we have

$$\mathbf{p}_p(t) = \mathbf{T}_c(t)C(s) \quad (2)$$

In addition, the initial position of the follower ball center \mathbf{p}_p at time $t = 0$ is known, i.e., $\mathbf{p}_p(0) = C(0)$.

Since the follower ball center \mathbf{p}_p is also a point on the follower, $\mathbf{p}_p(t)$ and $\mathbf{p}_p(0)$ have to satisfy the motion constraint enforced by the follower support (e.g., equal distance to the rotation center \mathbf{p}_s for camMech_2R; see Figure 6). This gives us the following equation:

$$G(\mathbf{T}_c(t)C(s), C(0)) = 0 \quad (3)$$

Please refer to the supplementary material for a list of Equation 3 for each class of camMechs.

At any given time t , we solve Equation 3 to obtain the parameter s . By this, we obtain the follower ball center position $\mathbf{p}_p(t)$. Since the motion type of the follower is known, its transformation matrix $\mathbf{T}_f(t)$ can be easily derived based on the position of a point before and after the transform (i.e., $\mathbf{p}_p(0)$ and $\mathbf{p}_p(t)$). Once we have the transformation matrix $\mathbf{T}_f(t)$, we could further compute the follower's (angular) velocity and (angular) acceleration at time t by taking derivatives.

End-effector trajectory. Given the follower transformation matrix $\mathbf{T}_f(t)$, the end-effector point \mathbf{p}_e 's position at time t can be represented as $\mathbf{p}_e(t) = \mathbf{T}_f(t)\mathbf{p}_e(0)$; see Figure 6. However, this representation does not explicitly show a relation between \mathbf{p}_e 's trajectory and the pitch curve $C(s)$. Hence, we choose another way to represent $\mathbf{p}_e(t)$. We know that the end-effector point \mathbf{p}_e and the follower ball center \mathbf{p}_p are both on the follower, and \mathbf{p}_p 's position at time t can be obtained by Equation 2. Hence, $\mathbf{p}_e(t)$ can be represented as:

$$\mathbf{p}_e(t) = \mathbf{L}\mathbf{T}_c(t)C(s), \quad t \in [0, T], s \in [0, 1] \quad (4)$$

where \mathbf{L} is a constant matrix, and s is a function of t , i.e., $s = s(t)$, computed based on Equation 3. Note that $s(0) = 0$ due to our way of parameterizing $C(s)$.

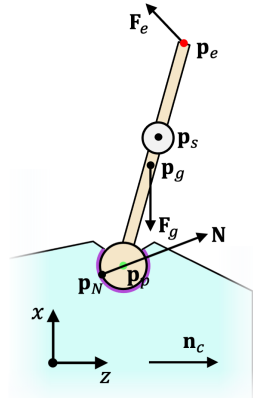


Fig. 8. Forces applied on the follower to make it rotate around the ball joint center \mathbf{p}_s , including the workload \mathbf{F}_e , gravity \mathbf{F}_g , and supporting force \mathbf{N} exerted by the 3D cam.

4.3 Dynamic Modeling

Assume that the cam's angular acceleration $\alpha_c(t)$ is known at any time $t \in [0, T]$. Based on the kinematic modeling, we can compute the follower acceleration $\mathbf{a}_f(t)$ and/or angular acceleration $\alpha_f(t)$. Assume that a workload applied on the follower's end-effector \mathbf{p}_e at time t is known and denoted as $\mathbf{F}_e(t)$. The goal of dynamic modeling is to compute a torque $\tau_c(t)$ required to drive the cam (e.g., by a motor) such that the cam and the follower can move with the known accelerations under the workload $\mathbf{F}_e(t)$. In other words, the dynamics of a camMech can be modeled as a function:

$$\tau_c(t) = D(\alpha_c(t), \mathbf{a}_f(t), \alpha_f(t), \mathbf{F}_e(t)), \quad t \in [0, T] \quad (5)$$

Note that Equation 5 is a simplification of real dynamics since we ignore friction and do not model tolerance. Despite this simplification, our computed τ_c provides a meaningful measure of a given camMech's dynamic performance under a known workload.

We compute $\tau_c(t)$ based on Newton's Second Law. At any time $t > 0$, we model the actual cam-follower contact as a point \mathbf{p}_N on the ball-move-in-groove joint. The supporting force exerted from the cam to the follower at point \mathbf{p}_N is denoted as \mathbf{N} ; see Figure 8. Our approach is to first solve \mathbf{p}_N and \mathbf{N} by applying Newton's Second Law on the follower. Based on the result, we can compute $\tau_c(t)$ by applying Newton's Second Law on the cam. Please refer to the supplementary material for details.

Remark. The role of our dynamic modeling is to efficiently quantify different designs of a camMech for geometry optimization instead of precisely simulating a given camMech's dynamic behavior. In particular, our dynamic modeling aims to identify camMechs with poor dynamic performance caused by the geometric design, no matter what kind of material is used for fabrication. This poor dynamic performance typically happens when the cam cannot push the follower effectively due to a large pressure angle. Our dynamic modeling without friction is able to identify these undesirable camMech designs and further help to avoid them in the optimization-based design process; see Section 6.

5 COMPOSITE CAM-FOLLOWER MECHANISMS

In this section, we first introduce a method to connect a pair of camMechs, and then describe an approach to combining multiple camMechs into a working C-camMech.

5.1 Connecting a pair of camMechs

Given a pair of camMechs M_i and M_j as shown in Figure 9, we denote the cam and the follower of M_i as c_i and f_i respectively. The condition of connecting M_i and M_j to form a working mechanism is that only component parts with the same motion type can be merged to form a new part. By this, the connected mechanism still can transfer motion and its kinematics can be derived from those of M_i and M_j . According to this condition, there are two ways of connecting M_i and M_j :

(i) *Multiple connection*. We assume 3D cams always have the same motion type, which is 1-DOF rotation. Hence, two 3D cams, c_i and c_j , can be merged to form a single driving part denoted as p_k . To achieve this, we first align M_i and M_j such that the rotation axis of c_i and c_j is co-linear. Next, we extract the two grooves of c_i and c_j , and construct the geometry of p_k as a new cam with the two grooves. In the resulting mechanism, the new part p_k can drive the motions of two followers, i.e., f_i and f_j ; see Figure 9 (top).

(ii) *Chain connection*. Chain connection makes use of camMech_1R (see Table 1 and Figure 4 (c)) since its follower has the same motion type (i.e., 1-DOF rotation) as the 3D cams. Without loss of generality, we assume M_i is a camMech_1R. By this, f_i and c_j can be merged to form a single part that is driven by c_i and drives f_j ; see Figure 9 (bottom). To achieve this, we first align M_i and M_j such that the rotation axes of f_i and c_j is co-linear. Next, we simply merge f_i and c_j to form a new part p_k . In the resulting mechanism, the two connected camMechs M_i and M_j form a motion transfer chain, where M_i is a parent camMech and M_j is a child camMech. This motion transfer chain allows adjusting the pose of the output motion by the follower f_j relative to the driving cam c_i flexibly. For example, the angle between the follower f_j 's motion axis and the driving cam c_i 's rotation axis is 90° in Figure 9 (bottom right), which cannot be achieved by deviating the follower motion axis v_s in a single camMech; see also Figure 7.

In the both ways of connecting two camMechs M_i and M_j , M_j has two degrees of freedom when aligned with M_i . The first DOF is a translation of M_j along the aligned axis, denoted as d_{align} . The second DOF is a rotation of M_j around the axis, denoted as ϕ_{align} . The connected mechanism's layout is determined by these two parameters.

5.2 Modeling C-camMechs

Multiple cam-follower mechanisms are possible to be combined into a working C-camMech based on the above two connection strategies. Since these combined camMechs eventually will be driven by a single motor, we define a motor mechanism, or simply *motorMech*, whose driver is the rotor and follower is the output shaft. We organize a motorMech and multiple camMechs into a tree structure, called *camMech tree*, in which each node is a motorMech or camMech, each edge represents a chain connection, and a sibling relation indicates a multiple connection. In a camMech tree, the root node is always the motorMech and the intermediate nodes have to be camMech_1R; see Figure 10 (a) and (b).

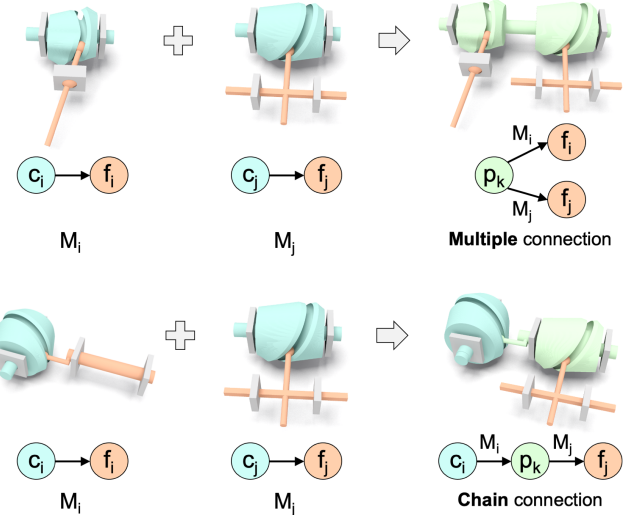


Fig. 9. Two different ways to connect a pair of camMechs M_i and M_j . (Top) Multiple connection where a new cam p_k drives two followers f_i and f_j . (Bottom) Chain connection where the cam c_i drives a new follower p_k , which further drives another follower f_j .

Geometric modeling. Based on the camMech tree, we can connect all the component camMechs by performing the chain connection operation iteratively in a breadth-first order. By this, each parent mechanism's follower will be merged with all the drivers (i.e., 3D cams) of its children to form a new part. For example, the follower of M_1 (i.e., the output shaft of the motor) will be merged with the two cams of M_2 and M_3 to form a new part, denoted as p_1 . The result of these connection operations is a working C-camMech that can be represented by a *part tree*, in which each node is a mechanical part and each edge corresponds to a node in the camMech tree; see Figure 10 (c) and (d). In other words, the part tree can be considered as a dual of the camMech tree.

Kinematic modeling. The part tree also can be interpreted as a *motion transfer tree* since we can simply replace each node from a part to its associated motion. Modeling kinematics of the resulting C-camMech is equivalent to computing the motion of each leaf node in the motion transfer tree, assuming the motion of the root node is known. Given a camMech M_i , we denote its motion transfer function as: $T_{f_i} = K_i(T_{c_i})$, where T_{c_i} is the transform of the cam and T_{f_i} is the transform of the follower, at any time t . Note that we can compute K_i independently for each camMech M_i based on the kinematic modeling approach in Section 4.2. Hence, to compute the motion of a leaf node, we can compose the involved motion transfer functions from the root all the way to the leaf node. For example, the motion of the leaf node f_4 in Figure 10 (c) and (d) should be $T_{f_4} = K_4(K_3(K_2(K_1(T_{d_1})))$, where T_{d_1} is the transform of the motor's output shaft.

Dynamic modeling. The goal of dynamic modeling is to compute a motor torque required to drive the whole C-camMech under known workloads at any time t . Given a camMech M_i , we denote its dynamic modeling function as: $\tau_{c_i} = D_i(F_{f_i})$, where F_{f_i} is the force applied on the follower f_i and τ_{c_i} is the required

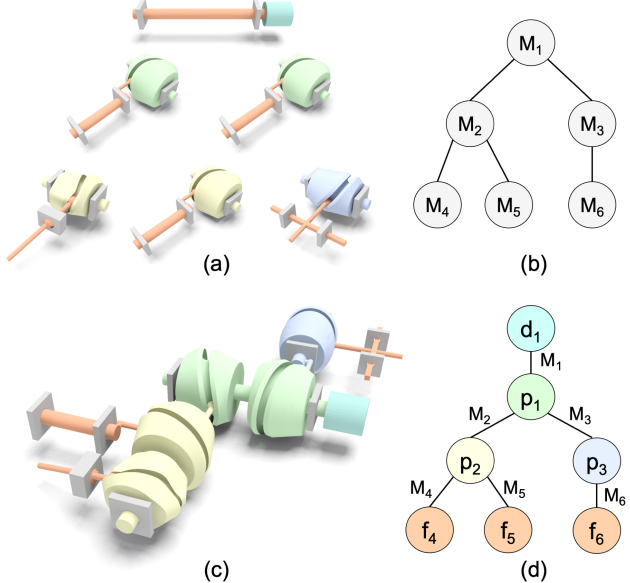


Fig. 10. Given (a) a motorMech and five camMechs, we represent them as (b) a camMech tree to guide their connection. The result is (c) a working C-camMech that can be represented as (d) a part tree. Note that 3D cams (a) before and (c) after the connection are rendered in the same color to indicate correspondence.

torque to drive the cam c_i . For simplicity, we omit the motion parameters in the function D_i ; see Equation 5. The required motor torque denoted as τ_{d_1} can be computed by accumulating the required torques in the part tree from the leaves all the way to the root. For the example shown in Figure 10 (c) and (d), we have $\tau_{d_1} = D_1(D_2(D_4(F_{f_4}) + D_5(F_{f_5})) + D_3(D_6(F_{f_6})))$.

6 DESIGN AND OPTIMIZATION

This section presents our approach to optimizing a C-camMech such that the five high-level requirements in Section 3 can be satisfied. In particular, we formulate the first two requirements on kinematics as hard constraints and the remaining three requirements as energy terms in the objective function. To facilitate understanding, we first present our approach to optimizing a camMech (Section 6.1), and then a C-camMech with multiple camMechs (Section 6.2).

6.1 Design of a camMech

To design a camMech with a known type, our input is a closed, smooth parametric curve $Q(u)$, $u \in [0, 1]$ in the world coordinate system, as well as the motion timing requirement specified as key points $\{p^l\}$ and time intervals $\{T^l\}$, $1 \leq l \leq n$; see again Figure 5. We compute a bounding sphere of the curve $Q(u)$, and denote its center as c_q .

Search space. The input curve $Q(u)$'s geometry indicates the follower-support joint pose in the world space. Taking camMech_2R in Figure 4 (f) as an example, the input curve $Q(u)$ is on a spherical surface centered at point p'_s . This sphere center p'_s exactly defines the follower-support joint position in the world space. We choose vector $v'_s = c_q - p'_s$ to define the follower-support joint orientation

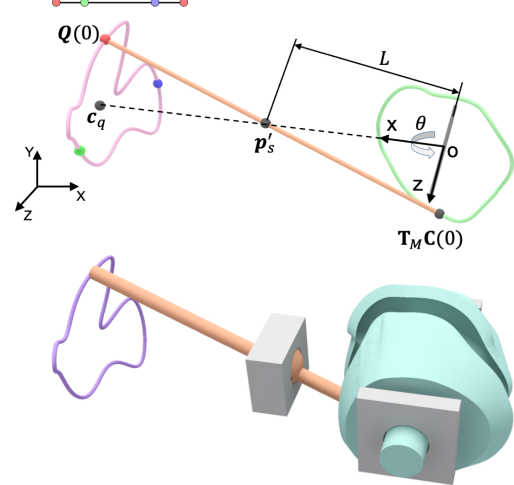


Fig. 11. (Top) Given an input curve $Q(u)$ (in magenta) as well as three key points and three time intervals, we design a camMech_2R whose follower-support joint is at point p'_s and follower is initially oriented along direction $Q(0) - p'_s$. Our search space includes the camMech's pose defined by L and θ , and the pitch curve (in green). (Bottom) Our optimized result, where the actual trajectory of the follower's end-effector (in purple) is exactly the same as the input curve $Q(u)$.

in the world space. The follower's initial pose is defined by the point p'_s and the end-effector's initial position $Q(0)$; see Figure 11 (top). The camMech's pose P is defined by its local coordinate frame in the world space. We define that the local frame's $+x$ -axis is along the vector v'_s , and the origin is on the ray from point p'_s along direction $-v'_s$. Our search space x includes:

- (1) A distance L that defines the camMech's origin on the ray in the world space.
- (2) An angle θ that defines the camMech's orientation in the world space, i.e., rotation around the camMech's x -axis.
- (3) Pitch curve $C(s)$, where $s \in [0, 1]$, defined in the camMech's local space.

Other parameters of the camMech are either predefined (e.g., the follower ball radius R) or calculated automatically according to the range of the follower motion (e.g., parameters $\{J_{\text{geom}}\}$ that define the geometry of the follower-support joint).

Objective function. Our design problem is formulated as minimizing the following objective function:

$$E(x) = \lambda_1 E_{\text{torq}}(x) + \lambda_2 E_{\text{weig}}(x) \quad (6)$$

$$\begin{aligned} E_{\text{torq}} &= \max_{t \in [0, T]} (|\tau_c(t)|), \\ \text{and } E_{\text{weig}} &= \text{Length}(C(s)), \end{aligned}$$

where $E_{\text{torq}}(x)$ is the largest torque required to drive the camMech during a whole motion period T , $E_{\text{weig}}(x)$ approximates the camMech's weight based on the length of the pitch curve $C(s)$, and λ_1 and λ_2 are weights of the two energy terms. Quantifying E_{torq} requires to simulate the camMech's dynamics for a whole motion period T . Without loss of generality, we assume the cam rotates with a constant angular speed at any time $t \in [0, T]$.

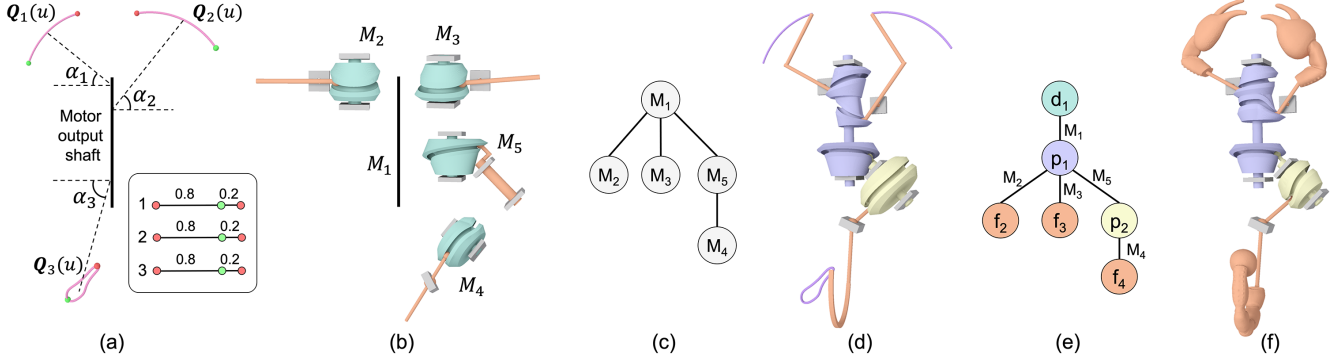


Fig. 12. Design of a C-camMech for a mechanical toy SCORPION. (a) Given three target curves, corresponding key points and time intervals, as well as the motor output axis, we first select (b) component camMechs and organize them as (c) a camMech tree, and then connect the component camMechs to form (d) an initial C-camMech that is represented as (e) a part tree. (f) Lastly, we optimize the C-camMech’s geometry and layout to minimize the objective function.

Constraints. We formulate the various constraints related to the fabrication and output motion as follows:

- (1) *Smooth cam groove.* The pitch curve $C(s)$ should be closed and smooth such that the resulting cam groove allows the follower ball to move periodically and smoothly in it (see Section 4.1):

$$\begin{aligned} C(0) &= C(1) \\ 1/\kappa(s) &> \zeta R, \quad s \in [0, 1] \end{aligned} \quad (7)$$

where $\kappa(s)$ is the curvature of $C(s)$, R is the follower ball radius, and ζ is a coefficient typically set as 1.2 in our experiments.

- (2) *Motion type.* The follower motion type should satisfy the constraint enforced by the follower support. This constraint is described by Equation 3.
- (3) *Motion trajectory.* The follower end-effector’s trajectory should be exactly the same as the input curve $Q(u)$:

$$T_M L T_c(t) C(s) = Q(u), \quad t \in [0, T], \quad s \in [0, 1] \quad (8)$$

where the left-hand side is the actual trajectory of the end-effector point p_e in the world space, and matrix T_M represents a transform from the camMech local space to the world space. See also Equation 4.

- (4) *Motion timing.* The follower end-effector’s motion should exactly follow the timing requirement specified by the key points $\{p^l\}$ and the time intervals $\{T^l\}$:

$$T_M L T_c(t^l) C(s(t^l)) = p^l, \quad \text{for each } l \in [1, n] \quad (9)$$

where $t^l = \sum_{j=1}^l T^j \cdot T$, and $s(t)$ is an unknown function of time t .

- (5) *Cam-follower contact.* Since the cam should always drive the motion of the follower, the cam’s velocity should be always larger than the follower’s velocity at the follower ball center $p_p(t)$:

$$|\omega_c \times p_p(t)| > |v_p(t)|, \quad t \in [0, T]$$

where the cam’s angular velocity $|\omega_c| = 2\pi/T$, the follower ball center’s position $p_p(t) = T_c(t) C(s)$ and velocity $v_p(t) = \frac{dp_p(t)}{dt}$.

Solver. The motion trajectory constraint (Equation 8) describes an analytical relation between the pitch curve $C(s)$ and the input curve $Q(u)$. The left and right sides of the equation are two different ways to represent the same curve. However, there are two parameters on the left side, which are s and t . To derive the pitch curve $C(s)$ based on the equation, we need to remove one parameter by finding a relation between s and t , i.e., $s(t)$. We choose to represent this unknown function $s(t)$ as a cubic spline, and initialize it as $s(t) = t$. By this, our new search space becomes the parameters L and θ , and the control points of $s(t)$. In our experiments, we choose 10 to 30 control points according to the target curve’s shape complexity. Increasing the number of control points further will slightly improve the objective function value, at the cost of higher computational complexity; please refer to the supplementary material for details. We discretize all the constraints with respect to the time t , and use a gradient-based method (i.e., the method of moving asymptotes (MMA) [Svanberg 1987]) to solve the optimization. Figure 11 (bottom) shows an optimized camMech by our approach.

6.2 Design of a C-camMech

To design a C-camMech with multiple camMechs, our input includes m target curves $\{Q_k(u)\}$, the timing control requirement specified as n_k key points $\{p_k^l\}$ and time intervals $\{T_k^l\}$, $1 \leq l \leq n_k$ for each curve $Q_k(u)$, as well as the pose of the motor’s output shaft in the world space; see Figure 12 (a). We assume the motor performs a rotational motion uniformly at any time t .

Given the above inputs, we first determine the topology of the C-camMech M . Our problem is similar to [Song et al. 2017] but relatively simple since the C-camMech contains only a few camMechs $\{M_i\}$, represented as a camMech tree. In particular, the root node of the tree is a motorMech and the type of each leaf node can be derived from the corresponding target curve according to Table 1 (e.g., a target curve on a spherical surface indicates a camMech_2R as the leaf node); see the root and leaf nodes in Figure 12 (b) and (c). For each target curve $Q_k(u)$, we compute a deviation angle α_k for the leaf node, which is the angle between the actual follower motion axis and its default one; see Figures 7 and 12 (a). If $\alpha_k < \alpha_{\text{thres}}$, we connect the leaf node directly with the root node; see M_2 and M_3 in Figure 12 (b) and (c). Otherwise, we insert one intermediate

node (i.e., camMech_1R) between the root node and a leaf node to form a chain connection, where the deviation angle α_k is equally distributed to the intermediate and leaf nodes; see M_5 inserted between M_1 and M_4 in Figure 12 (b) and (c).

Search space. The search space includes the parameters defined for each camMech M_i denoted as $\{L_i, \theta_i, C_i(s)\}$ (see Section 6.1), as well as parameters $\{d_{\text{align}}, \phi_{\text{align}}\}$ for aligning each child camMech with its parent during the connection.

Objective function. Our design problem is formulated as minimizing the following objective function:

$$E(\mathbf{x}) = \lambda_1 E_{\text{torq}}(\mathbf{x}) + \lambda_2 E_{\text{weig}}(\mathbf{x}) + \lambda_3 E_{\text{dim}}(\mathbf{x}) \quad (10)$$

$$\text{with } E_{\text{torq}} = \max_{t \in [0, T]} (|\tau_c(t)|),$$

$$E_{\text{weig}} = \sum_i \text{Length}(C_i(s)),$$

$$\text{and } E_{\text{dim}} = \text{Volume}(\text{BBox}(\{T_{M_i} C_i(s)\}, \{T_{M_i} p_s^i\})),$$

where $\tau_c(t)$ is the motor torque required to drive the C-camMech at time t , E_{weig} approximates the mechanism's weight using the pitch curves $\{C_i(s)\}$, E_{dim} approximates the mechanism's dimension using the pitch curves $\{C_i(s)\}$ and the follower-support joint positions $\{p_s^i\}$, and λ_1 , λ_2 , and λ_3 are weights of the energy terms.

Constraints. Each camMech M_i should satisfy the five constraints described in Section 6.1. In addition, collision among different camMechs should be avoided when the C-camMech M is in motion at any time $t \in [0, T]$. This constraint is satisfied by enforcing sufficient distance among all pitch curves $\{C_i(s)\}$ and all the follower-support joints centered at $\{p_s^i\}$ in the world space.

Solver. Solving Equation 10 requires optimizing not only the geometry but also layout of the C-camMech due to the energy term E_{dimen} . However, the collision-free constraint in the layout optimization is not differentiable with respect to the design parameters $\{d_{\text{align}}, \phi_{\text{align}}\}$. Hence we use an iterative method to solve the optimization problem.

We first fix the layout (i.e., $\{d_{\text{align}}, \phi_{\text{align}}\}$), and use the above gradient-based method to optimize each camMech M_i (i.e., search $\{L_i, \theta_i, C_i(s)\}$) to satisfy all the objectives in Equation 10 except E_{dim} . In case a camMech M_i is connected with the motor through a camMech_1R (see again Figure 10), both camMechs will be optimized together to satisfy Equations 8 and 9. Next, we fix the geometry of each component camMech M_i , and optimize the C-camMech M 's layout by searching $\{d_{\text{align}}, \phi_{\text{align}}\}$ using a randomized algorithm (i.e., improved stochastic ranking evolution strategy). Due to the small search space, this randomized search can be performed very efficiently. We iterate the above two steps until the decrease of energy $E(\mathbf{x})$ is sufficiently small. Figure 12 shows an example of our optimized C-camMech.

7 RESULTS

We implemented our tool in C++ and libigl [Jacobson et al. 2018] on a MacBook with a 1.4GHz CPU and 4GB memory, and employed NLOpt package [Johnson 2020] for solving our gradient-based optimizations. We have conducted experiments to evaluate

Table 2. Statistics of the results shown in this paper.

Fig	Automata	# cam Mech	# end-effector	# part	Optim. camMech Pose	Optim. Time (min)
1 (lef)	Drawing Machine	1	1	2	No	0.8
12	Scorpion Toy	4	3	5	Yes	11.2
13 (lef)	Star	1	1	2	No	0.3
13 (mid)	Star	1	1	2	No	0.5
13 (rig)	Star	1	1	2	No	0.6
14	T-Rex	1	1	2	No	0.4
15 (lef)	Leaf	1	1	2	Yes	1.0
15 (mid)	Leaf	1	1	2	Yes	1.1
15 (rig)	Leaf	1	1	2	Yes	1.4
16	Dove	1	1	2	No	0.4
17	camMech_1T	1	1	2	No	0.3
18	camMech_2T	1	1	2	No	0.3
19 (top)	Boxer Toy	3	3	4	Yes	7.2
19 (bot)	Frog Toy	5	4	6	Yes	13.5
20 (lef)	Car	1	1	2	No	0.5
20 (mid)	Cats	1	1	2	No	0.9
20 (rig)	Elephant	1	1	2	No	0.8
21	Walking Robot	6	6	7	No	4.4

our optimization-based design approach in different aspects (Figures 13, 14, 15, 16, 17, and 18), and used the approach to design a number of C-camMechs for different kinds of personalized automata, including drawing machines, mechanical toys, and walking robots (see Figures 1, 12, 19, 20, and 21). Please watch the accompanying video for demos. Table 2 presents statistics of all the results shown in the paper. The second to seventh columns from the left show basic information about the results: result name, number of camMechs, number of end-effectors, and number of mechanical parts (excluding support parts), whether the pose of each component camMech is optimized or fixed, and optimization time. Overall, optimizing a single camMech takes less than 1 min while optimizing a C-camMech takes from 4.4 mins to 13.5 mins. Fixing the pose of each camMech will significantly reduce the computation time due to the reduced search space.

Evaluation of timing control. We conducted an experiment to evaluate the impact of the timing control requirement on our designed camMechs. To this end, we generate three camMech_2R designs,

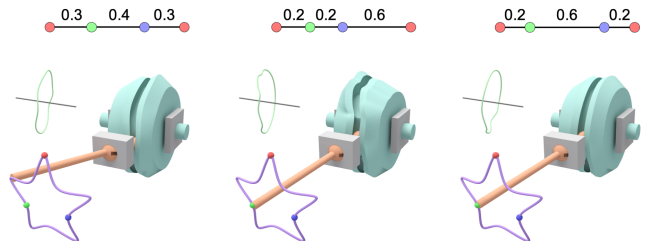


Fig. 13. Experiment to evaluate timing control. Given the same input curve and key points but different timing intervals, our optimization generates three camMech_2R designs, whose pitch curves have very different shapes. We show all the three camMechs at $t = 0.2T$.

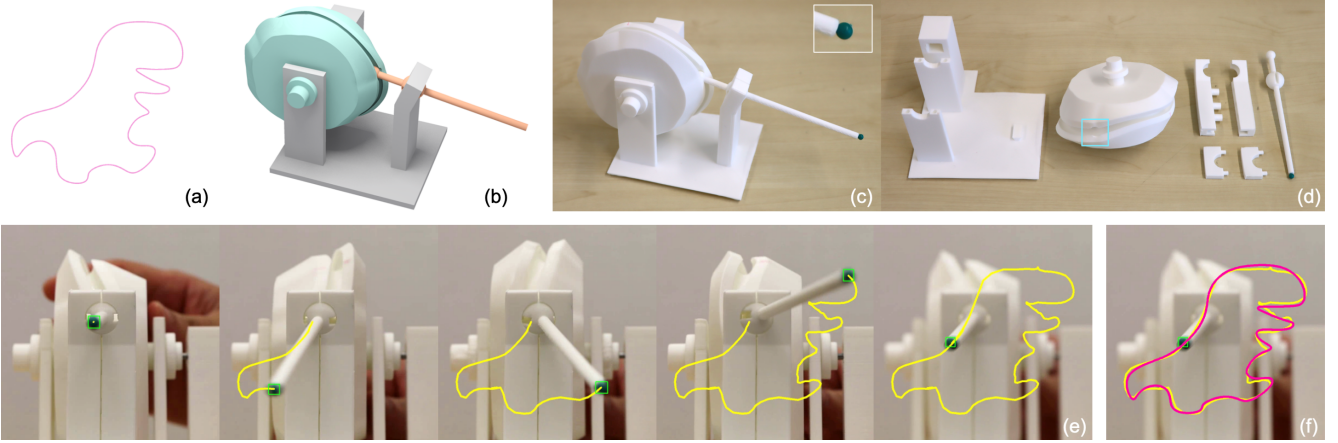


Fig. 14. Experiment to evaluate the kinematic performance for realizing a target curve T-Rex. (a) The target curve; (b) our designed camMech_2R; (c) and (d) 3D printed camMech and its component parts, where a small green ball is used as the follower end-effector; (e) tracking the green ball in the video images (see the green rectangles); and (f) comparing the tracked curve (in yellow) and the target curve projected onto the image (in magenta).

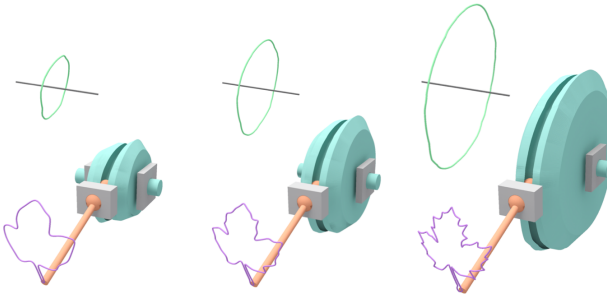


Fig. 15. Experiment to evaluate trajectory control. Given a target curve with different levels of details, our optimization generates three camMech_2R designs, whose pitch curves have very different sizes. We show all the three camMechs at $t = 0$.

taking as input the same curve $Q(u)$ and key points $\{p^l\}$ but different time intervals $\{T^l\}$; see Figure 13. We fix the pose of each camMech and optimize the pitch curve to satisfy the timing requirement. We observe that the timing requirement significantly affects the pitch curve's shape. In general, for a segment between two key points on the input curve, shorter timing requires a shorter segment on the pitch curve yet with high curvature to control the motion. Our simulated result shows that the timing requirement can be exactly satisfied by our designed camMechs. Please watch the accompanying video for demos.

Evaluation of trajectory control. We conducted an experiment to evaluate the impact of the trajectory control requirement on our designed camMechs. Hence, we take a target curve with three different levels of details as our input, and use our optimization to generate three camMech_2R designs respectively; see Figure 15. The timing requirement is ignored in this experiment. We observe that the more geometric details the input curve has, the larger the 3D cam is (i.e., the longer the pitch curve is). This is because the pitch curve needs to support reproducing geometric details in the input curve (Equation 8) while maintaining low curvature at any point (Equation 7).

Evaluation of kinematic performance. We conducted two physical experiments to evaluate the kinematic performance of our camMechs. The first experiment takes a T-REX curve while the second one takes a DOVE curve, as input; see Figures 14 and 16 and the accompanying video. For both experiments, we designed a camMech_2R to realize the target curve without any timing constraint, and fabricated it using an FDM 3D printer with 0.1mm accuracy, where the cam, follower, and support parts are 3D printed separately and assembled to form the mechanism. Male and female joints are constructed on the support parts for assembly purpose, whose tolerance is set as 0.06mm such that the support parts can be connected tightly. Tolerance of the cam-follower, cam-support, and follower-support joints is set as 0.25mm to encourage the movement of the cam and follower. A small opening is created on the cam groove for assembling the follower ball; see the cyan square in Figure 14 (d).

In the first experiment, we visualize the follower trajectory using an image processing technique. In detail, we use a video camera

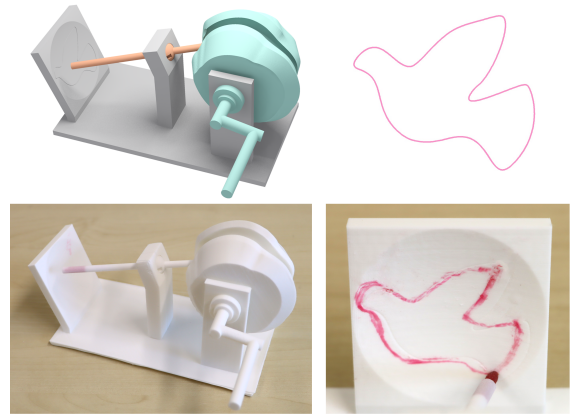


Fig. 16. Experiment to evaluate the kinematic performance for realizing a target curve Dove. (Top) A camMech_2R optimized by our approach, and the input curve. (Bottom) A 3D printed result, and the drawn curve.

to record the motion of the camMech for a whole motion period, and track the follower end-effector in the video images using the OpenCV library [OpenCV 2021]. To facilitate the image-based object tracking, we 3D printed the camMech using white material and used a small green ball as the follower end-effector. Figure 14 (e) shows the process to track the green ball and the resulting tracked curve. To compare our tracked curve with the target one quantitatively, we project the 3D target curve from the world space to the video image space based on the calibrated camera projection matrix. Figure 14 (f) shows the comparison result, where the Hausdorff distance between the two curves is 18.6 pixels. Given that the bounding box of the projected curve is 652×541 pixels with a diagonal of 847 pixels, the normalized Hausdorff distance is $18.6/847 = 2.2\%$. This relatively small difference between the two curves can be caused by inaccuracy introduced in fabrication, assembly, and/or object tracking.

In the second experiment, we visualize the follower end-effector's trajectory by drawing it on a spherical wall. To compare the drawn curve with the target one, we encode the target curve on the wall, and 3D print the wall and the cam support base as a single piece. We use a marker tip as the follower end-effector to record the actual trajectory on the wall. Figure 16 (bottom) shows the 3D printed

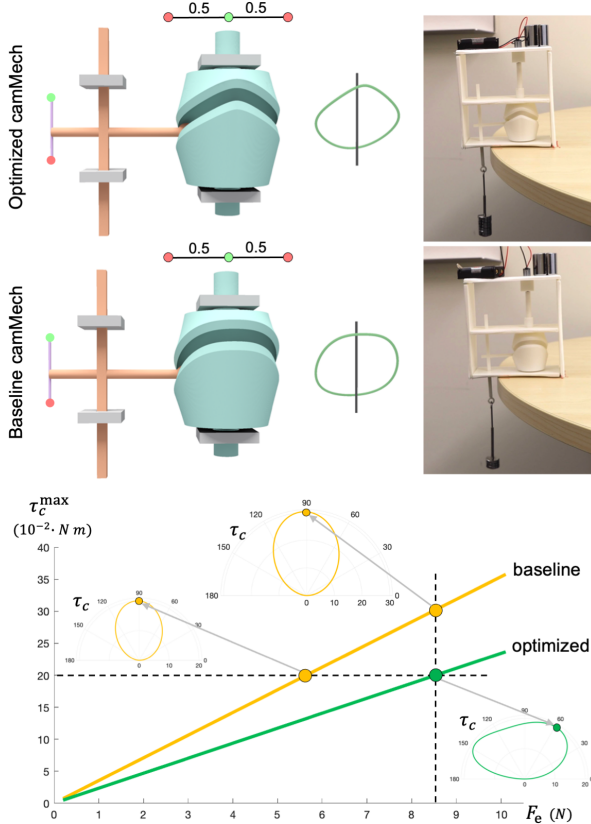


Fig. 17. Experiment to validate dynamic performance. (Top) A camMech_2R optimized by our approach, its pitch curve, and the fabricated result that can drive at most 60g weights. (Middle) A camMech_2R generated by a baseline approach, its pitch curve, and the fabricated result that can drive at most 25g weights. (Bottom) Compare the dynamic performance of the two camMechs according to our simulation.

camMech and the drawn result, from which we can see that the drawn curve is very close to the input one. Compared with the first experiment, the dynamic condition in this experiment is more complex since the wall exerts a reaction force on the follower during the drawing process. Despite this external force, our camMech still can realize the target curve properly, demonstrating its robustness.

Evaluation of dynamic performance. To evaluate the dynamic performance of our designed camMechs, we compare an optimized camMech_1T with a baseline design that is randomly generated to simply satisfy the constraints in Section 6.1.

Figure 17 shows the two camMechs, as well as their dynamic performance represented as a relation between the workload F_e and the maximum motor torque $\tau_c^{\max} = \max_{t \in [0, T]} (|\tau_c(t)|)$. The relation is linear since we assume geometry and kinematics are all fixed in the dynamic function; see Equation 5. In particular, the cam's angular acceleration is set as $\alpha_c(t) = 0$ for any time t . Given the same τ_c^{\max} , the optimized camMech can drive a workload F_e that is 56% larger than the baseline camMech. Figure 17 (bottom) visualizes $|\tau_c(t)|, t \in [0, 0.5T]$ for three points in the relation curves. We only visualize $|\tau_c(t)|$ for a half period since a motor torque is required only when lifting the weights (i.e., from the red key point to the green key point).

To verify the simulated result, we 3D printed the two camMechs, and a common support frame. During the experiment, we keep each camMech running driven by the same motor and batteries, and gradually increase the weights on the follower's end-effector. The experiment terminates until the camMech stops its motion caused by the workload that is too large to be driven by the motor. Due to the difficulty in measuring real accelerations, this physical experiment actually evaluates the camMechs' quasi-static performance. Since the follower has a very small acceleration, this measured quasi-static performance can be considered as a good approximation of the real dynamic performance. In this experiment, we observe that the optimized camMech can drive 60g weights while the baseline camMech can only drive 25g weights. Due to the self-weight of the follower and pothook (around 10g in total), the maximum workload that can be driven by the two camMechs is 70g and 35g respectively.

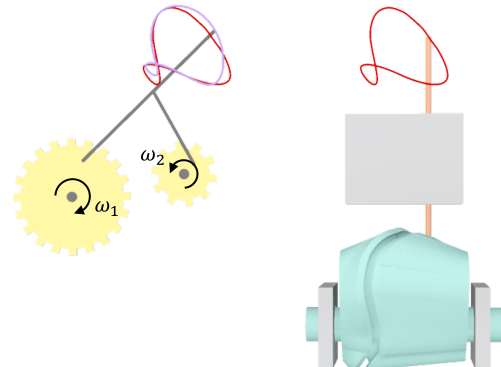


Fig. 18. Comparing (left) a five-bar linkage designed by Coros et al. [2013] with (right) a camMech_2T designed by our approach. Given a target curve (in red), the linkage can only approximate it (in purple) while our camMech can exactly follow it.

The ratio between the two maximum workloads, which is 2.0, is close to that (i.e., 1.56) predicted by our simulation. This result verifies the effectiveness of our optimization to make the camMech drivable by a small motor torque.

Comparison with Coros et al. [2013]. We compared our designed camMechs with linkage-based mechanisms designed by Coros et al. [2013]. To this end, we reproduced a five-bar linkage result shown in [Coros et al. 2013], which can only approximate a target curve; see Figure 18 (left). In contrast, our designed camMech_2T can exactly follow the target curve; see Figure 18 (right). In addition, the linkage has to be driven by two motors with synchronized angular speed (i.e., $\omega_2 = -2\omega_1$) while our camMech_2T can be driven by a single motor. Our advantage comes from the larger design space, i.e., the continuous pitch curve instead of a few joint parameters of the linkage. However, the larger design space also results in more bulky and complex geometry of the mechanism (i.e., the 3D cam), leading to more cost and higher demand on the fabrication. For example, the linkage can be fabricated cheaply and quickly with laser cutting while our camMechs can only be fabricated with 3D printing.

Drawing machines. Our designed camMechs (i.e., camMech_2T, camMech_1T1R, and camMech_2R) can be used as drawing machines. In Figure 16, we have used camMech_2R as a drawing machine to evaluate its kinematic performance. Figure 20 shows that our camMechs are able to draw complex, free-form curves on a 3D planar, cylindrical, or spherical surface, respectively. Our camMechs are suitable for drawing shapes whose boundary can be represented as a closed, smooth curve such as organic shapes. Our camMechs are able to draw curves with intricate geometric details, but the cost is that the 3D cam becomes larger; see again Figure 15. One potential application of these camMechs is to automate the drawing or painting on a cylindrical or spherical surface such as the interior of containers; see Figure 1 (left) for an example. This task cannot be achieved by conventional drawing machines based on gears and linkages [Roussel et al. 2017] since they draw on planar surfaces.

Mechanical toys. Our technique can be used to design mechanical toys with a variety of behavior; see Figure 1 (middle), 12, and 19. Thanks to the precise spatial-temporal motion control offered by our C-camMechs, we can design mechanical toys that perform realistic and interesting behavior by synchronizing motions of different end-effectors. The toy shown in Figure 12 mimics an attack by a SCORPION: move the pincers and tail slowly for preparation, and then move them quickly for an attack. For the BOXER toy shown in Figure 19 (top), we use two camMech_2Rs for controlling the motion of the boxer's fists, and one camMech_1O for the motion of the opponent. This toy mimics the motion of a boxing scenario: the boxer attacks with one fist while taking back the other; each of the two fists moves faster during attacking than being taken back; the opponent avoids the attack agilely by swinging his body; and the opponent even stops for a while when the boxer's fists are far away from him. The FROG toy shows an interesting animation: the frog attempts to catch a bug but fails, and then the bug moves to a reed; see Figure 19 (bottom). We use a camMech_2R to control the spatial motion of the bug on a sphere to make it look natural. A camMech_1T

is used to control the frog's tongue while a camMech_1O for controlling its mouth. The motion of the reed is controlled by another camMech_1O. Please watch the accompanying video for demos.

Walking robot. We have used our approach to design a 6-leg robot that walks following a user-specified gait. The gait is defined by six curves that represent trajectories of the legs, as well as corresponding timing requirement (e.g., move slowly when touching the ground and quickly when in the air); see Figure 21 (top left). In detail, the three legs on one side have been assigned three key points with time intervals $\{1/3, 1/3, 1/3\}$ while the three legs on the other side have four key points with time intervals $\{1/6, 1/3, 1/3, 1/6\}$. To ensure equilibrium of the robot during walking, the position of each key point on the curve has been carefully adjusted such that there are always at least 4 legs touching the ground (i.e., end-effector at the flat part of each curve) at any time. We design a C-camMech with six camMech_2Rs, where each camMech drives one leg; see Figure 21 (bottom left). To ensure that the robot can be driven by a micromotor, we optimize the C-camMech with a large weight on the energy term E_{torq} in Equation 10. To verify whether our designed robot can walk, we 3D printed it using an assembly-based approach similar to fabricating the two prototypes in Figures 14 and 16. We used a single geared DC motor (with 100 RPM rotation speed) to drive the mechanism, and installed it at one end of the robot. To facilitate smooth walking, we used lubricating oil to reduce friction in the 3D printed prototype. Figure 21 compares three real walking poses with those simulated poses, and we can see they are quite consistent. Please watch the accompanying video for a demo.

8 CONCLUSION

We presented a computational technique to model, design, and optimize composite cam-follower mechanisms for fabricating personalized automata. The strength of our C-camMechs include precise spatial-temporal motion control, complex motion on both planar and non-planar surfaces, and structural simplicity. We have demonstrated how these unique features enable functional behavior of personalized automata that cannot be easily achieved by conventional mechanisms, including walking robots following a user-specified gait, mechanical toys with realistic non-planar motion, and machines that can paint a bowl automatically.

Limitations and Future Work. Our work has several limitations that open up interesting directions for future research. First, our dynamic modeling does not consider friction, which may lead to a discrepancy between the simulation and real-world fabrication. We consider a systematic study of the camMech's dynamic behavior (e.g., under friction and even tolerance) as an important future work. Second, we have shown that our C-camMechs can perform complex spatial-temporal motion to achieve functional tasks. This capability can be further extended by combining our C-camMechs with other mechanisms such as linkages and non-circular gears [Xu et al. 2020]. More advanced methods such as evolutionary algorithms can be employed to search for the topology of this class of combined mechanisms. Third, our design approach optimizes for the trajectory and timing of the output motion. Taking velocity and even acceleration into consideration would be helpful for using our C-camMechs in

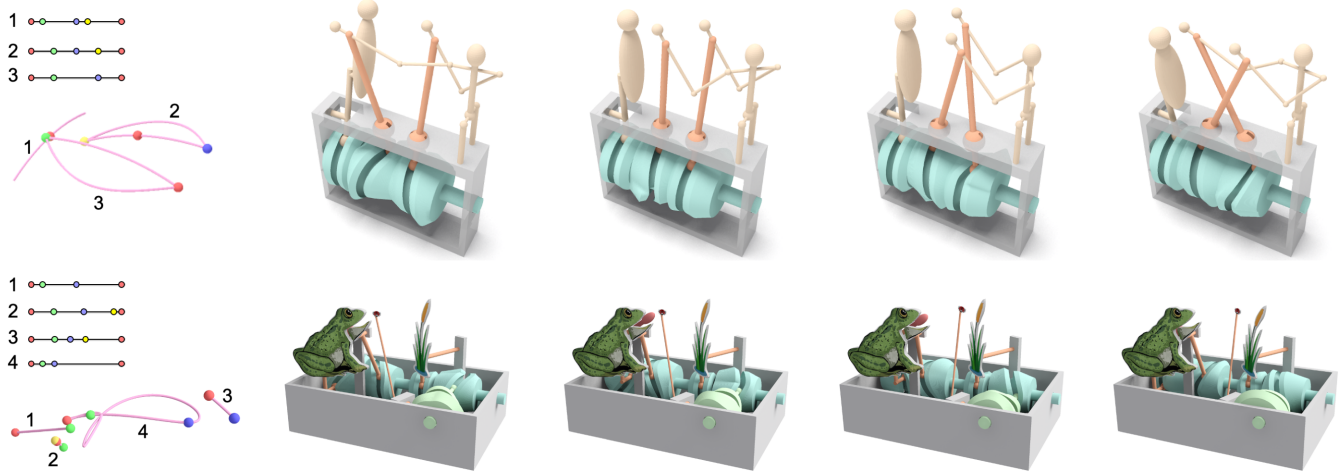


Fig. 19. Two mechanical toys designed by our approach: (top) a BOXER in a fight and (bottom) a FROG catching a bug. The user input is shown on the left.

mechanical engineering. Last but not least, there are many potential applications of our C-camMechs in the field of robotics due to their capacity of precise motion control, e.g., legged locomotion with gait transition [Mannhart et al. 2020], eyeball control mechanism [Khan and Chen 2018], and robotic grasping [Song et al. 2018].

ACKNOWLEDGMENTS

We thank the reviewers for their valuable comments. This work was supported by the SUTD Start-up Research Grant (Number: SRG ISTD 2019 148), the National Natural Science Foundation of China (62025207), and Zhejiang Lab (NO. 2019NB0AB03).

REFERENCES

- Hammoudi Abderazek, Ali Riza Yildiz, and Seyedali Mirjalili. 2020. Comparison of Recent Optimization Algorithms for Design Optimization of a Cam-follower Mechanism. *Knowledge-Based Systems* 191 (2020). Article no. 105237.
- Moritz Bächer, Stelian Coros, and Bernhard Thomaszewski. 2015. LinkEdit: Interactive Linkage Editing using Symbolic Kinematics. *ACM Trans. on Graph. (SIGGRAPH)* 34, 4 (2015), 99:1–99:8.
- C J Backhouse and J Rees Jones. 1990. Envelope Theory Applied to Globoidal Cam Surface Geometry. *Journal of Mechanical Engineering Science (Proc. the Institution of Mechanical Engineers)* 204, 6 (1990), 409–416.
- Duygu Ceylan, Wilmot Li, Niloy J. Mitra, Maneesh Agrawala, and Mark Pauly. 2013. Designing and Fabricating Mechanical Automata from Mocap Sequences. *ACM Trans. on Graph. (SIGGRAPH Asia)* 32, 6 (2013), 186:1–186:11.
- Zongyu Chang, Changmi Xu, Tongqing Pan, Lei Wang, and Xichao Zhang. 2009. A General Framework for Geometry Design of Indexing Cam Mechanism. *Mechanism and Machine Theory* 44, 11 (2009), 2079–2084.
- Stelian Coros, Bernhard Thomaszewski, Gioacchino Noris, Shinjiro Sueda, Moira Forberg, Robert W. Sumner, Wojciech Matusik, and Bernd Bickel. 2013. Computational Design of Mechanical Characters. *ACM Trans. on Graph. (SIGGRAPH)* 32, 4 (2013), 83:1–83:12.
- S. G. Dhande, B. S. Bhadaria, and J. Chakraborty. 1975. A Unified Approach to the Analytical Design of Three-dimensional Cam Mechanisms. *Journal of Engineering for Industry* 97, 1 (1975), 327–333.
- M. A. González-Palacios and J. Angeles. 1994. The Generation of Contact Surfaces of Indexing Cam Mechanisms – A Unified Approach. *Journal of Mechanical Design* 116, 2 (1994), 369–374.
- Jean Hergel and Sylvain Lefebvre. 2015. 3D Fabrication of 2D Mechanisms. *Comp. Graph. Forum (Eurographics)* 34, 2 (2015), 229–238.
- G S Hwang and D M Tsay. 2009. Profile Surfaces of Cylindrical Cams with Arbitrarily-shaped Followers. *Journal of Mechanical Engineering Science (Proc. the Institution of Mechanical Engineers)* 223, 8 (2009), 1943–1953.
- Alec Jacobson, Daniele Panozzo, et al. 2018. libigl: A simple C++ geometry processing library. <https://libigl.github.io/>.
- Steven G. Johnson. 2020. The NLOpt nonlinear-optimization package. <http://github.com/stevengj/nlopt>.
- Masood M Khan and Cheng Chen. 2018. Design of A Single Cam Single Actuator Multiloop Eyeball Mechanism. In *Proc. IEEE-RAS 18th International Conference on Humanoid Robots (Humanoids)*. 1143–1149.
- Panagiotis N. Koustoumpardis, Sotiris Smyrnis, and Nikos A. Aspragathos. 2017. A 3-Finger Robotic Gripper for Grasping Fabrics Based on Cams-Followers Mechanism. In *Proc. International Conference on Robotics in Alpe-Adria Danube Region*. 612–620.
- Mimin Lin, Tianjia Shao, Youyi Zheng, Niloy Jyoti Mitra, and Kun Zhou. 2018a. Recovering Functional Mechanical Assemblies from Raw Scans. *IEEE Trans. Vis. & Comp. Graphics* 24, 3 (2018), 1354–1367.
- Mimin Lin, Tianjia Shao, Youyi Zheng, Zhong Ren, Yanlin Weng, and Yin Yang. 2018b. Automatic Mechanism Modeling from a Single Image with CNNs. *Comp. Graph. Forum (Pacific Graphics)* 37, 7 (2018), 337–348.
- Dominik Mannhart, Fabio Dubois, Karen Bodie, Victor Klemm, Alessandro Morra, and Marco Hutter. 2020. CAMI - Analysis, Design and Realization of a Force-Compliant Variable Cam System. In *Proc. IEEE Int. Conf. on Robotics and Automation*. 850–856.
- Vittorio Megaro, Bernhard Thomaszewski, Damien Gaigne, Eitan Grinspun, Stelian Coros, and Markus Gross. 2014. ChaCra: An Interactive Design System for Rapid Character Crafting. In *Proc. ACM SIGGRAPH/Eurographics Symp. on Computer Animation*. 123–130.
- Vittorio Megaro, Jonas Zehnder, Moritz Bächer, Stelian Coros, Markus Gross, and Bernhard Thomaszewski. 2017. A Computational Design Tool for Compliant Mechanisms. *ACM Trans. on Graph. (SIGGRAPH)* 36, 4 (2017), 82:1–82:12.
- Niloy J. Mitra, Yong-Liang Yang, Dong-Ming Yan, Wilmot Li, and Maneesh Agrawala. 2010. Illustrating How Mechanical Assemblies Work. *ACM Trans. on Graph. (SIGGRAPH)* 29, 4 (2010), 58:1–58:11.
- OpenCV. 2021. Open Source Computer Vision Library. <https://opencv.org/>.
- Rodney Peppé. 2002. *Automata and Mechanical Toys*. Crowood Press.
- Robin Roussel, Marie-Paule Cani, Jean-Claude Léon, and Niloy J. Mitra. 2017. SPIROU: Constrained Exploration for Mechanical Motion Design. In *Proc. ACM Symposium on Computational Fabrication*. 7:1–7:11.
- Robin Roussel, Marie-Paule Cani, Jean-Claude Léon, and Niloy J. Mitra. 2018. Exploratory Design of Mechanical Devices with Motion Constraints. *Comp. & Graph. (Computational Fabrication)* 74 (2018), 244–256.

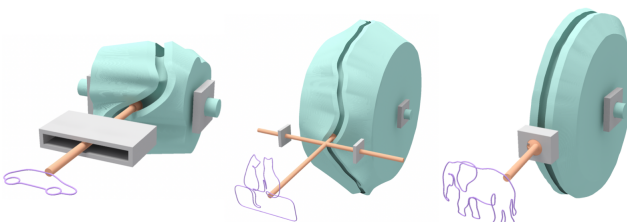


Fig. 20. Three camMechs designed by our approach for drawing (left) CAR, (middle) CATS, and (right) ELEPHANT.

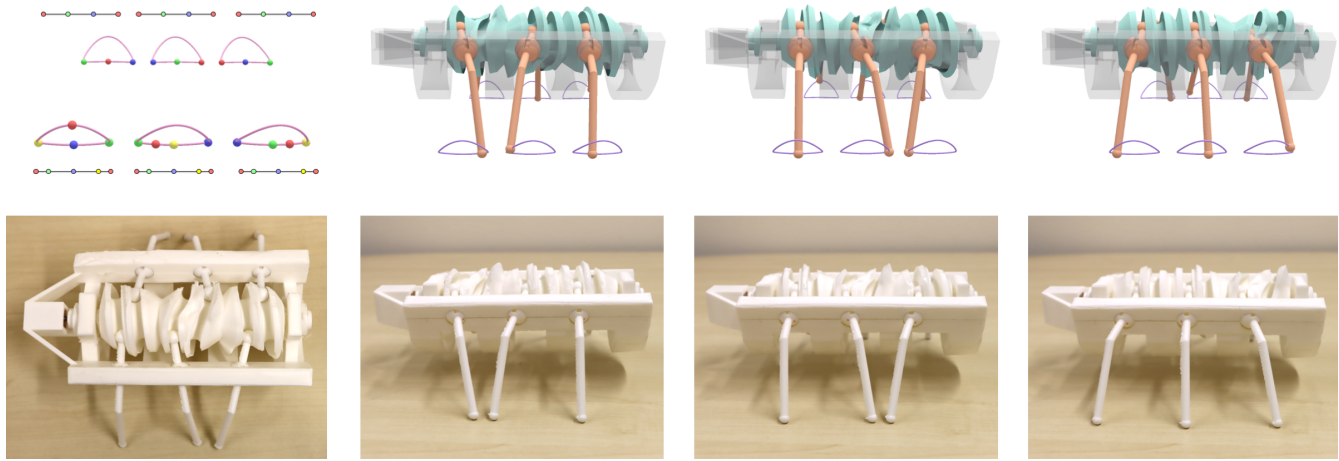


Fig. 21. A 6-leg walking robot designed by our approach. (Top) The user input and three samples of simulated walking poses. (Bottom) Our 3D printed result and three walking poses.

- Peng Song, Zhongqi Fu, and Ligang Liu. 2018. Grasp Planning via Hand-Object Geometric Fitting. *The Visual Computer* 34, 2 (2018), 257–270.
- Peng Song, Xiaofei Wang, Xiao Tang, Chi-Wing Fu, Hongfei Xu, Ligang Liu, and Niloy J. Mitra. 2017. Computational Design of Wind-up Toys. *ACM Trans. on Graph. (SIGGRAPH Asia)* 36, 6 (2017), 238:1–238:13.
- Hiroshi Sugihara. 2016. Ready to Crawl. Finalist of YouFab Global Creative Awards, <https://www.youfab.info/2016/winners/ready-to-crawl>.
- Krister Svanberg. 1987. The Method of Moving Asymptotes – A New Method for Structural Optimization. *Internat. J. Numer. Methods Engrg.* 24, 2 (1987), 359–373.
- Takuto Takahashi and Hiroshi G. Okuno. 2018. Design and Implementation of Programmable Drawing Automata based on Cam Mechanisms for Representing Spatial Trajectory. In *Proc. IEEE/RSJ Intl. Conf. on Intelligent Robots and Systems*. 450–455.
- Pengbin Tang, Jonas Zehnder, Stelian Coros, and Bernhard Thomaszewski. 2020. A Harmonic Balance Approach for Designing Compliant Mechanical Systems with Nonlinear Periodic Motions. *ACM Trans. on Graph. (SIGGRAPH Asia)* 39, 6 (2020), 191:1–191:14.
- Bernhard Thomaszewski, Stelian Coros, Damien Gauge, Vittorio Megaro, Eitan Grinspun, and Markus Gross. 2014. Computational Design of Linkage-Based Characters. *ACM Trans. on Graph. (SIGGRAPH)* 33, 4 (2014), 64:1–64:9.
- Der-Min Tsay and Guan Shyong Hwang. 1994. Application of the Theory of Envelope to the Determination of Camoid Profiles with Translating Followers. *Journal of Mechanical Design* 116, 1 (1994), 320–325.
- D M Tsay and B J Lin. 1996. Profile Determination of Planar and Spatial Cams with Cylindrical Roller-followers. *Journal of Mechanical Engineering Science (Proc. the Institution of Mechanical Engineers)* 210, 6 (1996), 565–574.
- Der-Min Tsay and Sheng-Yang Lin. 2006. Generation of Globoidal Cam Surfaces With Conical Roller-Followers. In *ASME International Design Engineering Technical Conferences & Computers and Information in Engineering Conference*. Paper No. DETC2006-99683.
- Der-Min Tsay and Hsien Min Wei. 1996. A General Approach to the Determination of Planar and Spatial Cam Profiles. *Journal of Mechanical Design* 118, 2 (1996), 259–265.
- Francisca Gil Ureta, Chelsea Tymms, and Denis Zorin. 2016. Interactive Modeling of Mechanical Objects. *Comp. Graph. Forum (SGP)* 35, 5 (2016), 145–155.
- Hao Xu, Tianwen Fu, Peng Song, Mingjun Zhou, Chi-Wing Fu, and Niloy J. Mitra. 2020. Computational Design and Optimization of Non-Circular Gears. *Comp. Graph. Forum (Eurographics)* 39, 2 (2020), 399–409.
- Hongyi Xu, Espen Knoop, Stelian Coros, and Moritz Bächer. 2018. Bend-It: Design and Fabrication of Kinetic Wire Characters. *ACM Trans. on Graph. (SIGGRAPH Asia)* 37, 6 (2018), 239:1–239:15.
- Mingliang Xu, Mingyuan Li, Weiwei Xu, Zhigang Deng, Yin Yang, and Kun Zhou. 2016. Interactive Mechanism Modeling from Multi-view Images. *ACM Trans. on Graph. (SIGGRAPH Asia)* 35, 6 (2016), 236:1–236:13.
- Lifeng Zhu, Weiwei Xu, John Snyder, Yang Liu, Guoping Wang, and Baining Guo. 2012. Motion-Guided Mechanical Toy Modeling. *ACM Trans. on Graph. (SIGGRAPH Asia)* 31, 6 (2012), 127:1–127:10.